Numerical investigation of an advanced U-RANS based pressure fluctuation model to simulate non-linear vibrations of nuclear fuel rods due to turbulent parallel-flow

Kottapalli, S.; Shams, A.; van Zuijlen, Alexander; Pourquie, M. J.B.M.

DOI
10.1016/j.anucene.2019.01.001

Publication date
2019

Document Version
Final published version

Published in
Annals of Nuclear Energy

Citation (APA)
Kottapalli, S., Shams, A., van Zuijlen, A., & Pourquie, M. J. B. M. (2019). Numerical investigation of an advanced U-RANS based pressure fluctuation model to simulate non-linear vibrations of nuclear fuel rods due to turbulent parallel-flow. *Annals of Nuclear Energy*, *128*, 115-126. https://doi.org/10.1016/j.anucene.2019.01.001

Annals of Nuclear Energy 128 (2019) 115–126

Contents lists available at ScienceDirect

Annals of Nuclear Energy

journal homepage: www.elsevier.com/locate/anucene

Numerical investigation of an advanced U-RANS based pressure fluctuation model to simulate non-linear vibrations of nuclear fuel rods due to turbulent parallel-flow

S. Kottapalli [a], A. Shams [a,*], A.H. Zuijlen [b], M.J.B.M. Pourquie [b]

[a] Nuclear Research and Consultancy Group (NRG), Petten, The Netherlands
[b] Delft University of Technology, Delft, The Netherlands

ARTICLE INFO

Article history:
Received 20 October 2018
Received in revised form 29 December 2018
Accepted 3 January 2019
Available online 9 January 2019

Keywords:
Flow induced vibrations
Fluid–structure interaction
Nuclear reactors
U-RANS
Pressure fluctuation modeling
Turbulent flows

ABSTRACT

Nuclear reactor designs such as PWR and BWR are susceptible to vibrations induced on the nuclear fuel rods due to fast flowing coolants around the rods. The non-linear behaviour of flexible components have always been a challenge to compute especially when dealing with strongly coupled fluid–structure interaction cases as found in the reactors. Simulating such a behaviour involves a two-way coupling of a well resolved turbulent flow Computational Fluid Dynamics (CFD) solver to a Computational Solid Mechanics (CSM) solver. The use of a high fidelity CFD solver to resolve turbulent flows in an FSI (Fluid-Structure Interaction) simulation is computationally expensive ergo is not practical in for industrial purposes. To address this issue, a different approach is discussed in this article to simulate turbulence induced vibrations through the use of U-RANS models. The method is based on computing the modeled turbulent pressure and velocity fluctuations from values obtained by solving U-RANS (Unsteady-Reynolds Averaged Navier Stokes) equations. The calculated turbulent fluctuating field is combined with mean values to compute an instantaneous turbulent pressure field to apply an external pressure and shear force on the structure and vice-verse until convergence is achieved. This method can be used to accurately estimate the behaviour of a flexible structure in a turbulent flow. The article provides a detailed explanation of the model followed by validation with three numerical test cases. The first case involves a CFD simulation where results from the pressure fluctuation model (PFM) is compared to a benchmark DNS (Direct Numerical Simulation) of a turbulent channel flow with friction Reynolds number, $Re_\tau = 640$. Later the PFM is applied to a 2-dimensional strongly-coupled FSI simulation with a flexible steel flap in turbulent water flow to study the feasibility and stability of PFM applied to an FSI problem. Finally, the PFM is used to simulate an experimental case of a brass rod excited by turbulent water performed by Chen and Wambsganns (1972). The results show that the PFM is capable of simulating turbulence induced vibration (TIV) with low-fidelity U-RANS models.

1. Introduction

Nuclear reactor designs such as the PWR (Pressurized Water Reactors) and BWR (Boiling Water Reactors) require on a constant flow of heavy or light water across the nuclear fuel rods to ensure proper cooling of the fuel rods and heat transfer to generate electricity. Due to dynamic coupling of turbulent flow of water within the reactors and the flexible structures, vibrations are induced on the fuel rods and measuring probes, also known as FIV (Flow Induced Vibrations) (Blevins, 1979; Païdoussis, 1983). FIV can reduce the service life of a structural component significantly and leading to failures like fatigue cracking and loosening of measuring probes. For extremely critical components such as in nuclear reactor cores, instabilities caused due to fluid flow on fuel rods are a high risk safety hazard. Further more, the issue of flow induced vibrations gets more serious in new reactor designs such as the MSR (Molten salt reactors) where extremely dense liquid fuel is circulated within the reactor for the nuclear reaction to sustain. In such conditions the behaviour of flexible structures are often non-linear and difficult to predict. Additionally, the dangerous and closed conditions within a reactor make it difficult or often impossible to measure the flow conditions in every section of the reactor. Hence it poses a huge challenge to estimate the real-time behaviour of the fluid and structures. Consequently, it

* Corresponding author.
E-mail address: shams@nrg.eu (A. Shams).

https://doi.org/10.1016/j.anucene.2019.01.001
0306-4549/

Nomenclature

$\boldsymbol{\kappa}$	Wave vector	ν	Kinematc viscosity
$\boldsymbol{\sigma}$	Unit vector	ν_t	Kinematc turbulent viscosity
ϵ	Turbulent energy dissipation rate	ω_n	Characteristic angular frequency at nth Fourier mode
κ_e	Wave number at which E is maximum	ρ	Density
κ_l	Kolmogorov wave number	τ_n	Kolmogorov time scale
κ_n	Wave number at nth Fourier mode	$\bar{u}_n$	Amplitude of the estimated turbulent velocity at nth Fourier mode
$\overline{\mathbf{p}}$	Ensemble averaged pressure		
$\overline{\mathbf{u}}$	Ensemble averaged velocity vector	E	Turbulent energy spectrum density
$\mathbf{u_c}$	Eddy convective velocity	k	Turbulent kinetic energy
$\mathbf{u}'$	Turbulent velocity vector	p'	Turbulent pressure

becomes necessary to estimate the behaviour of the fluid and structure either analytically or numerically.

Most modern nuclear reactor designs employ a parallel-flow design within nuclear reactors to maximize the efficiency of heat transfer which can be also be observed in the CFD study by Conner et al. (2010) for an existing PWR. In the study by Blevins (1979); Païdoussis, 1983, it is observed that the vibrations induced within reactors with parallel flow configurations are caused due to the pressure fluctuations that are observed during turbulent flow of fluids also known as TIV. Chen and Wambsganns (1972) in their study clearly depict a non-linear behaviour of metal rods when subjected to parallel-flows with increasing flow rates. Various studies by Païdoussis (1983), Païdoussis and Gagnon (1984), Païdoussis and Curling (1985), Chen and Wambsganns (1972) to estimate the effect of a turbulent flow on structures are validated for weak coupling between fluid and structure where the density ratios between fluids and structures are much less than 1. However, for strongly coupled cases analytic predictive models require extra parameters which are derived from experiments to calculate empirical constants (JSME, 2008). However, experimental studies on TIV due to parallel-flows are limited, which presents another complication when dealing with complex geometries. Hence numerical computations based on a two-way coupling between CFD and CSM solvers are necessary to ensure stability and accuracy of the solution of the fluid–structure FSI problem. For industrial purposes, using a high fidelity CFD such as DNS or LES (Large Eddy Simulation) in an FSI simulation is expensive. Ergo a pragmatic approach is used which makes use of U-RANS models to simulate turbulent flows.

The U-RANS models are widely popular in industries as an efficient way of computing properties of a turbulent flow. The U-RANS approach provides a time-dependent solution of RANS equations to compute average velocity, pressure, and the temperature of the fluid flow. The lower requirement of memory and computational power for these models makes them a popular choice for computation of flow through complicated geometries. A recent study by Santis et al. (2018) also shows that U-RANS is able to capture low frequency fluid elastic instabilities due to pressure differences of the flow outside and inside and the fuel rod assembly causing them to vibrate and form different mode shapes. However, U-RANS models compute the ensemble averages of stochastic quantities of a fluid flow. Therefore fluctuating quantities such as the turbulent velocities ($\mathbf{u}'$) and pressures (p') are not computed. Although U-RANS equations do take into account the isotropic part of the Reynolds shear stress of a turbulent flow while computing the mean quantities, the deviatoric part of the Reynolds shear stress is modeled as an additional viscosity term which acts in the tangential direction to the surface of the structure in an FSI simulation. As a result, the behaviour of the structure as predicted by a standard U-RANS equations so not take into account the changes in pressure caused due to interaction between eddies in a turbulent flow. Studies by ter Hofstede et al. (2017), de Ridder et al. (2013), Santis and Shams (2017), Santis and Shams (2019) to check the feasibility of U-RANS models for FSI simulations involving turbulent flows have shown that the results obtained are not representative of the actual behavior of a structure observed in a turbulent flows due absence of an excitation caused due to fluctuating pressures. The resulting vibrations due to U-RANS models are not sustained due to absence of external excitation. One way to resolve this, is by calculating the turbulent pressure fluctuations from the mean flow quantities and later impose them on the solid. This would result in a more physically representative behavior of the system.

Modeling of the turbulent pressure field has been performed in many studies using empirical correlations, statistical analysis and numerical simulations which have been mentioned by Juvé et al. (2014). The empirical model suggested by Chase (1980), Chase (1987) are based on many experimental results for flows with zero pressure gradients. Peltier and Hambric (2007) suggested a model to estimate the turbulent pressure spectrum from the values obtained from RANS simulations by formulating the co-variance of pressure fluctuations by using an appropriate Greens function. For a wall bounded turbulent flow, this process can become very complicated. Moreover, the results obtained are in the frequency domain which then have to be converted into a time domain signal, for an FSI simulation. A study by Senthooran (2002), Senthooran et al. (2004), provides a numerical approach to model the pressure signal in the time domain by modelling the turbulent velocity from the turbulent kinetic energy (k) and the turbulent dissipation rate (ϵ) obtained from RANS models. In the current study the turbulent quantities obtained from U-RANS models are used to calculate the turbulent velocity and pressures in space and time. The pressure signal on the walls of the fluid domain can be mapped on to the structural domain in an FSI simulation.

2. The Pressure Fluctuation Model (PFM)

As stated earlier, standard U-RANS models are not suitable for simulating TIV in an FSI simulation mainly due to the nature of the equations involved. In a U-RANS model the continuity, momentum and the transport equations of the turbulent kinetic energy (k) and turbulent dissipation rate (ϵ) to calculate the time dependent properties of a divergence free flow. The continuity equation in the set of equations can be written as,

$$\frac{\partial \overline{u_i}}{\partial x} = 0 \tag{1}$$

and the momentum transport equation as,

$$\frac{\partial \overline{u_i}}{\partial t} + \frac{\partial \overline{u_i u_j}}{\partial x_j} = -\frac{1}{\rho}\frac{\partial \overline{p}}{\partial x_i} - \frac{\partial}{\partial x_i}\left(-\nu\frac{\partial \overline{u_i}}{\partial x_j} + \overline{u_i' u_j'}\right) + f_i \tag{2}$$

Here, $\overline{u_i}$ is the mean velocity, ρ is the fluid density, t is the time, $\overline{p}$ is the mean pressure and f_i is the body force. The term $\overline{u_i'u_j'}$ is the Reynolds Stress tensor and ν is the kinematic viscosity of the fluid. Assuming that turbulence is isotropic in nature, the Reynolds stress tensor is modeled in terms of mean velocities by a hypothesis proposed by Boussinesq (Tennekes and Lumley, 1972; Pope, 2000; Hinze, 1975).

$$\overline{u_i'u_j'} = \nu_t\left(\frac{\partial\overline{u_i}}{\partial x_j}+\frac{\partial\overline{u_j}}{\partial x_i}\right)-\frac{2}{3}k\delta_{ij} \tag{3}$$

where, δ_{ij} is the Kronecker delta and ν_t is the turbulent kinematic viscosity which is modeled as

$$\nu_t = C\frac{k^2}{\epsilon} \tag{4}$$

here, k is the turbulent kinetic energy, ϵ is the energy dissipation rate and C is a empirical constant that is dependent on the U-RANS model selected. From the above equations it can noted that a U-RANS model computes ensemble averages. Hence, using U-RANS models directly in an FSI simulation can lead to erroneous results for example in the case of simulating TIV on flexible structures. PFM was introduced to address this issue. The PFM tries to model and estimate the turbulent velocity and pressure fields using mathematical models.

Early work has been performed in this regard to model the turbulent velocity (u') and pressure (p') using steady RANS models (Senthooran, 2002). The PFM calculates an unsteady fluctuating field using U-RANS models. Fig. 1 explains the difference between the working of a standard U-RANS model and PFM. Typically, the pressure fluctuation model is an additional post-processing that is performed on a standard U-RANS model before transferring the traction forces onto the solid solver. Every step involved in modeling of pressure fluctuations is explained more in detail further within this article.

2.1. Modeling the velocity fluctuations

The first step in PFM is the modeling of instantaneous turbulent velocity field $\mathbf{u}'$ which is later used to calculate the turbulent pressure field. The 3-dimensional fluctuating velocity field is expressed as a convolution of a periodic function and the amplitude of velocity amplitude with a finite number of Fourier modes. The total velocity fluctuation field is modeled as the summation of velocity fluctuations at each Fourier mode. The range of eddies in a turbulent regime is a continuous field which is discretized into a selected number of modes or wave numbers. This is represented by

$$\boldsymbol{u}'(\mathrm{x},t) = \sum_{n=1}^{N}\widetilde{u}_n\cos\left(2\pi\boldsymbol{\kappa}_n.(\mathbf{x}-t\mathbf{u}_c)+\psi_n\right)\sin\left(2\pi\omega_n t\right)\boldsymbol{\sigma}_n \tag{5}$$

where $\widetilde{u}_n$, is the amplitude, ψ_n, and ω_n are the phase, and the characteristic angular frequency, $\boldsymbol{\sigma}_n$ is the unit direction vector, and $\boldsymbol{\kappa}_n$ is the wave vector at nth Fourier mode respectively. The term $\mathbf{u}_c$ is the convective velocity of eddies.

In the above model of turbulence velocity field, the amplitudes are dependent on the turbulent kinetic energy at each Fourier mode, the periodic waves ensures that the ensemble and the time average of the function would be zero. The vector (σ_n) is the velocity vector to ensure that the field is divergence free. Finally the phase difference (ψ_n) is a function of Gaussian white noise which is introduced to generate a random field. Hence, to calculate the velocity field, every term is has to be calculated from the quantities obtained from U-RANS model.

2.1.1. Calculating the wave vector and the direction vector

The wave vector $(\boldsymbol{\kappa}_n)$ is defined as the inverse of the eddy length scale for each Fourier mode. Since these eddies are in a 3-dimensional space, the wave number is represented in the form of a wave vector. Similarly, the direction vector $(\boldsymbol{\sigma}_n)$ is a unit vector. Both these quantities namely, $\boldsymbol{\kappa}_n$ and $\boldsymbol{\sigma}_n$, are related to each other through continuity equation.

For an incompressible flow, the continuity equation for $\mathbf{u}'$ is given by,

$$\frac{\partial u_i'}{\partial x_i} = 0 \tag{6}$$

To satisfy the above condition, the Eq. (6) is applied to Eq. (5). From this it follows that, the necessary condition for satisfying both the equations is,

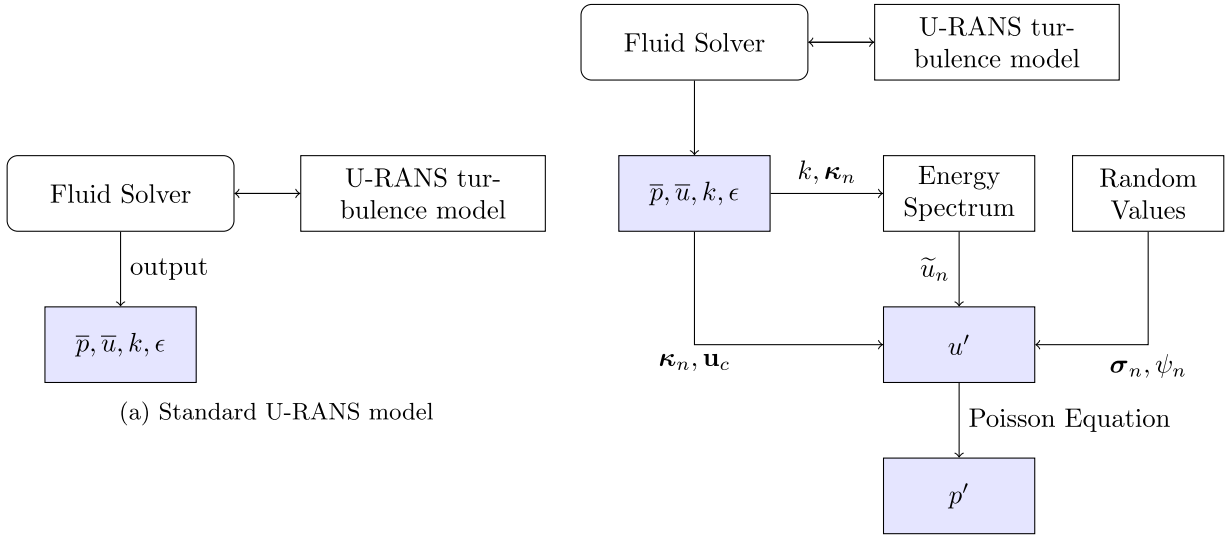

(a) Standard U-RANS model

(b) U-RANS with Pressure Fluctuation Model.

Fig. 1. Flowchart depicting differences in the work flow of 1a) the standard U-RANS model and 1b) the U-RANS model coupled with PFM. In Fig. 1b, it can be observed that the output from the standard U-RANS model is used to calculate a set of unknown parameters which are utilized to calculate the turbulent velocity and pressure fields. The blue boxes indicate the outputs of the solvers.

$$\boldsymbol{\kappa}_n \cdot \boldsymbol{\sigma}_n = 0, \quad n = 1, \ldots, N \tag{7}$$

This implies that the wave vector $\boldsymbol{\kappa}_n$ is orthogonal to the unit vector $\boldsymbol{\sigma}_n$ for any given mode. Considering the vector $\boldsymbol{\kappa}_n$ to lie in a 3-dimensional space with spherical coordinates $(\kappa_n, \phi_n, \theta_n)$, the Cartesian transform of the vector can be written as

$$\boldsymbol{\kappa}_n = \kappa_n\left[(\sin\theta_n \cos\phi_n)\kappa^1 + (\sin\theta_n \sin\phi_n)\kappa^2 + (\cos\theta_n)\kappa^3\right]$$

where κ_n is the magnitude of $\boldsymbol{\kappa}_n$ vector, and κ^i are the directions of in Cartesian coordinates. Similarly, assuming that the vector $\boldsymbol{\sigma}_n$ lies in a plane perpendicular to the wave vector $\boldsymbol{\kappa}_n$ (since the vectors are orthogonal). The direction vector $\boldsymbol{\sigma}_n$ can then be represented by spherical coordinates (1,α_n,0) with origin at the tip of the unit vector $\boldsymbol{\kappa}_n$, and in Cartesian coordinates by

$$\boldsymbol{\sigma}_n = \kappa^{1'} \cos\alpha_n + \kappa^{2'} \sin\ \alpha_n$$

where, $\kappa^{i'}$ are the directions in Cartesian coordinates with origin at the base of vector $\boldsymbol{\sigma}_n$. Now applying the orthogonality rule, the angle α_n can be calculated as

$$\alpha_n = \tan^{-1}\left(-\frac{1}{\cos\theta_n}\right)$$

For isotropic and homogeneous turbulence, the random variables ϕ_n, ψ_n and θ_n are calculated by using a random number generator in the following probability density functions (Senthooran, 2002),

$$\begin{aligned} &P(\phi_n) = \tfrac{1}{2\pi} \\ &P(\psi_n) = \tfrac{1}{\pi} \\ &P(\theta_n) = \tfrac{1}{2}\sin(\theta_n) \end{aligned} \tag{8}$$

The characteristic angular frequency ω_n is the frequency of the eddies of wave vector $\boldsymbol{\kappa}_n$ at each Fourier mode n. After the wave vectors calculations are complete, value of ω_n is calculated through Eq. (9) (Senthooran, 2002).

$$\omega_n = \epsilon^{1/3}\kappa_n^{2/3} \tag{9}$$

where, $\kappa_n = ||\boldsymbol{\kappa}_n||$

2.1.2. Estimating the Energy Spectrum

Fig. 1a shows that the amplitude $\widetilde{u}_n$ of the fluctuations at each Fourier mode is calculated from the energy spectrum for the respective mode. Hence, the next step in this direction is to estimate the turbulent energy spectrum for the flow. In a typical turbulent energy spectrum the maximum turbulent kinetic energy is contained by the length scales of the largest eddies which correspond to the smallest wave numbers. Therefore, this range is also known as the energy containing range. This is followed by the inertial subrange where energy contained decays proportional to $\kappa^{-5/3}$ (Tennekes and Lumley, 1972; Hinze, 1975). Finally, at the smallest eddy length scales which correspond to the largest wave numbers, energy is dissipated purely due to viscosity. These smallest eddy length scales are also known as the Kolmogorov scales. To model this complete behavior of the turbulent energy spectrum, the PFM employs a model suggested by Von-Karman to estimate the turbulent energy spectrum as a function of wave number κ_n. The model for the energy spectrum, $E(\kappa_n)$, for isotropic turbulence (Hinze, 1975) is shown below

$$E(\kappa_n) = 2^{17/6}E(\kappa_e)\frac{(\kappa_n/\kappa_e)^4}{\left[1+(\kappa_n/\kappa_e)^2\right]^{\frac{17}{6}}}\exp\left[-2\nu\kappa_n^2\tau_\eta\right] \tag{10}$$

where, κ_e is the wave number at which $E(\kappa_n)$ is maximum and τ_η is the Kolmogorov time scale calculated by

$$\tau_\eta = \left[\frac{\nu}{\epsilon}\right]^{1/2}$$

The value $E(\kappa_e)$ is approximated using the following equation (Hinze, 1975),

$$E(\kappa_e) = A\frac{k}{\Delta\kappa} \tag{11}$$

where A is a constant of the order unity, k is the total turbulent kinetic energy and

$$\Delta\kappa = \kappa_\eta - \kappa_l$$

where κ_l are the wave numbers corresponding to largest eddy length scales, and κ_η the Kolmogorov wave numbers. Each of them are calculated as,

$$\kappa_l = \frac{\epsilon}{\mathbf{u}^3} \text{ and } \kappa_\eta = \left[\frac{\epsilon}{\nu^3}\right]^{1/4}$$

In the Eq. (10), there are two unknowns A and κ_e which need to be calculated. It is known that in the inertial sub-range value of $E(\kappa)$ is calculated by the following equation (Hinze, 1975),

$$E(\kappa_n) = A\epsilon^{2/3}(\kappa_n)^{-5/3} \tag{12}$$

Further to calculate κ_e and A, Eq. (12) has to be satisfied. Since, viscosity effects are negligible in the inertial sub-range, the exponential term in Eq. (10) can be ignored and equated to Eq. (12) which results in,

$$A\epsilon^{2/3}\kappa_e^{-5/3}\left(\frac{\kappa_n}{\kappa_e}\right)^{-5/3} = 2^{17/6}E(\kappa_e)\frac{(\kappa_n/\kappa_e)^4}{\left[1+(\kappa_n/\kappa_e)^2\right]^{\frac{17}{6}}} \tag{13}$$

It is also known that in inertial sub-range $\kappa_n/\kappa_e \gg 1$. Therefore, applying this condition and substituting Eq. (11) in the above equation,

$$\kappa_e = 2^{-17/10}\left[\frac{\Delta\kappa}{k}\right]^{3/5}\epsilon^{2/5} \tag{14}$$

Hence, using the above equation, κ_e can be calculated. Here, by definition the turbulent kinetic energy can be calculated using the following equation,

$$k = \int_0^\infty E(\kappa_n)\ \mathrm{d}\kappa_n \tag{15}$$

Now, substituting Eq. (10) in Eq. (15) the value of A can be calculated as

$$A = \Delta\kappa\left[2^{17/6}\kappa_e\int_0^1 \frac{\zeta^{3/2}}{(1-\zeta)^{2/3}}\exp\left[-\beta\frac{\zeta}{(1-\zeta)}\tau_\eta\right]\mathrm{d}\zeta\right]^{-1} \tag{16}$$

where

$\beta = 2\nu\kappa_e^2$ and $\zeta \to R \in [0,1]$.

Since the value of κ_e is now known from Eq. (14), the value of A can be obtained from Eq. (16). After the unknown parameters κ_e and A are computed, the value of $E(\kappa_n)$ is computed for all the modes using Eq. (10). Also, from $\omega_n$and κ_e the magnitude of convective velocity is calculated by (Senthooran, 2002; Senthooran et al., 2004)

$$||\mathbf{u}_c|| = \frac{\omega_n}{\kappa_e} \tag{17}$$

The number of modes has to be selected by the user depending on the resolution of energy spectrum required. Higher number of modes gives a better approximation of the energy spectrum, however, it also increases the computational costs involved.

2.1.3. Calculating the amplitude

The amplitude $\widetilde{u}_n$ defines the magnitude of fluctuation at each mode or wave number. To estimate the amplitude at each Fourier

mode, the definitions of turbulent kinetic energy is put to use by equating the turbulent velocity in Eq. (5) and the energy spectrum in Eq. (15). In their discrete forms the equations would be as follows

$$\frac{1}{2}\sum_{i=1}^{N}\widetilde{u}_i^2\cos^2\Theta_i=\sum_{i=1}^{N}\frac{E(\kappa_i)\delta\kappa_i}{\frac{1}{2}\left[1-\frac{\sin(4\pi\omega_i t)}{4\pi\omega_i t}\right]} \tag{18}$$

where, N is the number of modes to be resolved, ω_i is the characteristic angular frequency, $\Theta_n=\boldsymbol{\kappa}_n.(\mathbf{x}-t\mathbf{u}_c)+\psi_n$, and $\delta\kappa_i$ is given by,

$$\delta\kappa_i=\kappa_1\left(e^{\Delta_l\kappa}-1\right)e^{[(i-1)\Delta_l\kappa]}$$

where,

$$\Delta_l\kappa=\frac{\log\kappa_N-\log\kappa_1}{N-1}$$

Finally, from Eq. (19) the velocity amplitude at all modes is calculated,

$$\widetilde{u}_n=\frac{1}{|\cos\Theta_i|}\left[\frac{E(\kappa_i)\delta\kappa_i}{\frac{1}{4}\left[1-\frac{\sin(4\pi\omega_i t)}{4\pi\omega_i t}\right]}\right]^{1/2} \tag{19}$$

Finally, substituting all the calculated unknowns in Eq. (5) the turbulent velocity field, $\boldsymbol{u}'_n$ can be calculated.

2.2. Calculating pressure fluctuation field

After the turbulent velocity field has been computed, the turbulent pressure field, (p') is computed. This is computed using the Poisson's equation (Juvé et al., 2014).

$$\frac{\partial^2 p'}{\partial x_i\partial x_i}=-\rho\left[2\frac{\partial\overline{u_i}}{\partial x_j}\frac{\partial u'_j}{\partial x_i}+\frac{\partial^2}{\partial x_i\partial x_j}\left(u'_iu'_j-\overline{u'_iu'_j}\right)\right] \tag{20}$$

2.3. Calculating the traction at the fluid–structure interface

In an FSI simulation, the fluid solver takes the displacements and the velocities of the mesh interface as the input and gives the traction as its output. In a standard U-RANS model, traction is calculated using the mean pressure $(\overline{p})$, and the wall shear stress (τ). In the pressure fluctuation model, the calculated pressure fluctuations (p') would be added to the mean pressure to calculate traction due to p'. It is done as follows,

$$\textit{Pressure Force}=\int(\overline{p}+p')\,dA \tag{21}$$

This ensures that the forces due to random pressure fluctuations are also transferred to the solid solver, leading to an external excitation condition.

3. Numerical code

To implement the complete method discussed above and perform the FSI simulation, two different codes were utilised. The fluid equations were solved using, OpenFOAM Extend v3.2. OpenFOAM Extend is a fork of OpenFOAM (OpenFOAM, 2013), which is an open source CFD package. OpenFOAM extend is contains libraries to discretize and solve equations using the Finite Volume method (FVM). Since the code is open source, the implementation of the PFM was easier with greater flexibility.

OpenFOAM Extend was externally coupled to a FEM (Finite Element method) package namely `Deal.II` (Arndt et al., 2017). `Deal.II` is a Finite Element library containing all the tools to discretize and solve partial differential equations using FEM.

4. Validating the pressure fluctuation model

To validate the PFM three test cases are performed. In the first test case a fluid only simulation is performed to validate the results of pressure fluctuation model with the results from a benchmark DNS. Consequently as a validation test case, DNS of turbulent plane channel flow with $Re_\tau=640$ performed by Abe et al. (2001) is selected. The second test case is a 2-dimensional FSI simulation of a flexible steel flap in turbulent water. The second test case is performed to check the feasibility and stability of the two-way coupling between the fluid solver employing PFM with a U-RANS model and the solid solver in a simulation involving fluid–structure interaction. The results are compared to an FSI simulation with fluid solver using a standard U-RANS model as a reference. To test the method further an application based experimental case by Chen and Wambsganns (1972) is simulated and compared to literature to validate the use of PFM.

4.1. Turbulent plane channel flow

The turbulent plane channel flow is a numerical benchmark case consisting of turbulent flow of an incompressible fluid bounded by two infinitely extending, smooth and flat parallel plates. The fluid domain mainly consists of a long rectangular channel to ensure no correlation between the values at the inlet to the outlet. The domain dimensions consists of a channel height of $H=2\delta$ and the length of the channel $L=8\pi\delta$. DNS of turbulent channel flows are extensively utilized as a benchmark for validating various turbulence models and high-fidelity solvers, ergo it is also selected for validating the results of PFM. The test case performed is validated with the DNS of a turbulent plane channel flow by Abe et al. (2001) with a friction Reynolds number of $Re_\tau=640$. The PFM uses the values of the turbulent kinetic energy (k) and turbulent dissipation rate (ω) calculated from the U-RANS equations to estimate turbulent pressure fluctuations through the method as explained in Section 2. The simulation set-up, mesh and boundary conditions for the simulation is explained further in detail.

4.1.1. Simulation set-up

The configuration, dimensions and mesh of the fluid domain are shown in Fig. 2. The fluid domain is two-dimensional, with the direction of fluid flow starting from the left side boundary face (inlet) towards the right side boundary of the fluid domain (outlet). The inlet and outlet of the domain connected with a translating cyclic boundary condition. The top and bottom of the mesh boundary are walls with no-slip boundary condition. The mesh is resolved such that the first cell thickness at the walls are kept at $y^+\leqslant 1$. The $k-\omega$ U-RANS model (Wilcox, 1988) is used to calculate the turbulent properties of the flow.

To start with the simulation, an initial steady-state RANS simulation is performed in order to ensure fully developed boundary layers at the walls. A momentum source term is applied on the fluid to maintain the fluid flow and the results are analyzed after convergence is achieved. The forcing term is calculated from the definition of u_τ.

$$u_\tau=\left[\frac{\tau_{wall}}{\rho_f}\right]^{1/2}$$

where, u_τ is the friction velocity and τ_{wall}, the wall shear stress. Once a steady-state is achieved, an unsteady simulation is performed for a total time of 150 s with the PFM enabled. A second order time stepping scheme is used and the time steps are maintained such that the Courant number for the flow is maintained $\leqslant 1$. The standard $k-\omega$ model is used to calculate the turbulent viscosity. Due

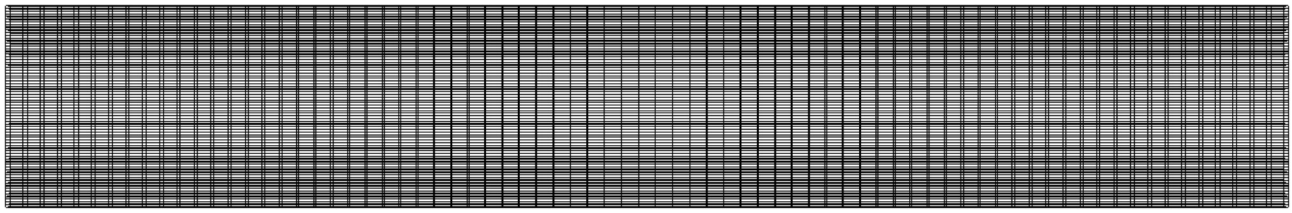

Fig. 2. Fluid domain for turbulent plane channel flow. The length of the domain, $L = 8\pi\delta$, and $H = 2\delta$. Here δ is the half channel width.

to a fully resolved mesh, use of wall function for turbulent kinetic energy (k) was not necessary. Whereas, a wall function for the turbulent dissipation rate (ω), is required at the walls to avoid floating point errors also known as the `omegaWallFunction` in OpenFOAM (2013). The results from the simulations are compared to the results by Abe et al. (2001). A summary of boundary conditions can be found in Table 1. The comparison between the k^+ plots of DNS and the U-RANS equations has been shown in Fig. 6. The results have been compared at the two different points at the center-line of the fluid domain.

- Position A: At the Wall.
- Position B: At Half-Channel height.

Table 1
Boundary conditions in OpenFOAM (2013) for the variables that were used for the Turbulent Channel Flow simulation using the $k-\omega$ U-RANS model.

Variable	Boundary	Boundary Condition
`U`	Walls	`noSlip`
	Inlet–Outlet	`cyclic`
`p`	Walls	`zeroGradient`
	Inlet–Outlet	`cyclic`
`k`	Walls	`fixedValue`
	Inlet–Outlet	`cyclic`
`omega`	Walls	`omegaWallFunction`
	Inlet–Outlet	`cyclic`

4.1.2. Results and discussion

Figs. 3 and 4 show an instantaneous pressure fluctuation and the velocity fluctuation field calculated from the PFM. Similarly, the pressure and velocity fluctuations for all the components at Point B (half channel width), have also been shown in Fig. 5a.

It is observed in the Figs. 3–5a that the velocity and pressure fluctuations show a fluctuating behavior around a mean value. It can be seen that PFM does a good job of achieving a fluctuating behaviour of turbulent flows. It satisfies the criteria of $\overline{p'} = 0$, which is the first objective of the pressure fluctuation model obtained from RANS and U-RANS equations. The second objective is to study the comparison between stochastic properties of modeled pressure fluctuations and DNS performed at $Re_\tau = 640$ by Abe et al. (2001). Table 2 compares the root mean square values of turbulent pressure field (p') and the average turbulent kinetic energy (k) at positions A and B. The values in Table 2 have been normalized using friction velocity u_τ.

To further analyze the fluctuating behaviour of the turbulent pressure field (p') obtained from the PFM, a comparison is done between DNS and PFM pressure signal. This is done by plotting the power spectrum density (PSD) as a function of wave number κ and comparing it to DNS data. The comparison plot can be observed in Fig. 5b. The PSD obtained from PFM conforms with the DNS results till wave numbers up to 10^2. After which the divergence can be seen from the reference data. Since, most of the energy in the spectra is contained in the lower wave numbers the effect of smaller eddy scales in the causing TIV is less signifi-

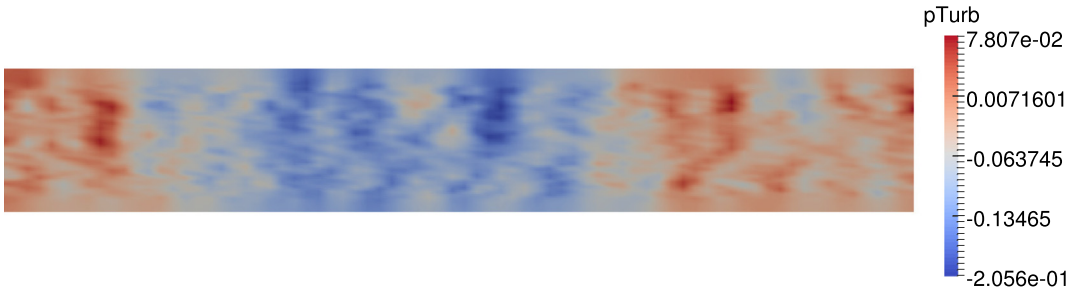

Fig. 3. Modeled pressure fluctuations from turbulence model. The values shown are in $\frac{m^2}{s^2}$.

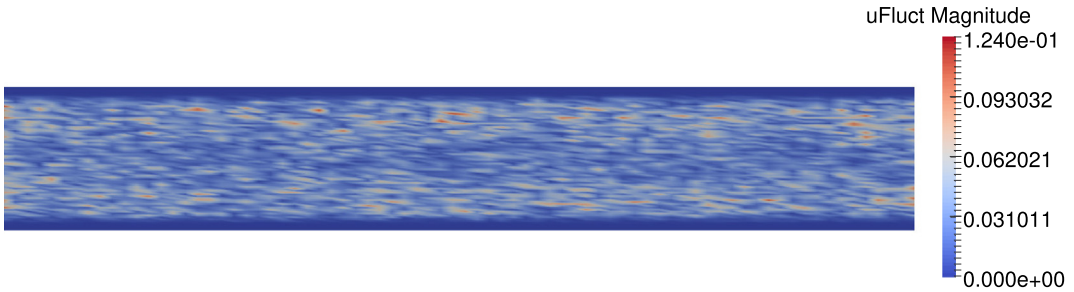

Fig. 4. Modeled velocity fluctuations from turbulence model. The values are in $\frac{m}{s}$.

Table 2
Comparison between the flow characteristics of DNS results and the results from U-RANS model with pressure fluctuation model.

$Re_\tau = 640$			
Case	Position	p'_{rms}	k
Abe et al. (2001)	Position A	2.26	0.0
PFM		1.11	0.0
$k-\omega$ model		0.000017	0.0
Abe et al., 2001	Position B	0.746	0.771
PFM		1.09	0.86
$k-\omega$ model		0.000019	0.86

cant. This can be verified by comparing the cumulative of the power spectral density for both cases in the Fig. 5b, given by

$$\Phi_{cum} = \int \Phi_{pp}(f)\ \delta f$$

The Φ_{cum} of DNS for the complete spectrum was calculated to be 5.85 $\left(\frac{Pa}{kg\ m^{-3}}\right)^2$ compared to 5.23 $\left(\frac{Pa}{kg\ m^{-3}}\right)^2$ for the PFM which gives an error percentage of 10%.

It is observed from the table that near the wall, root mean square (RMS) of the turbulent pressure is underestimated when compared to DNS. Whereas, at the center root mean square of turbulent pressure estimation is higher. This corresponds to the lower and higher estimation of the turbulent kinetic energy near the wall and the half-channel height respectively observed in Fig. 6. However, the RMS values of pressure fluctuations p' are in the same order of magnitudes when compared to DNS results when compared to the fluctuations in mean pressure values obtained standard U-RANS model. This implies that although there is a margin of error involved in the modeled pressure fluctuations the turbulent pressures estimated from PFM, the errors are significantly lower compared to standard U-RANS models and hence can be used as an external excitation for a coupled FSI simulation.

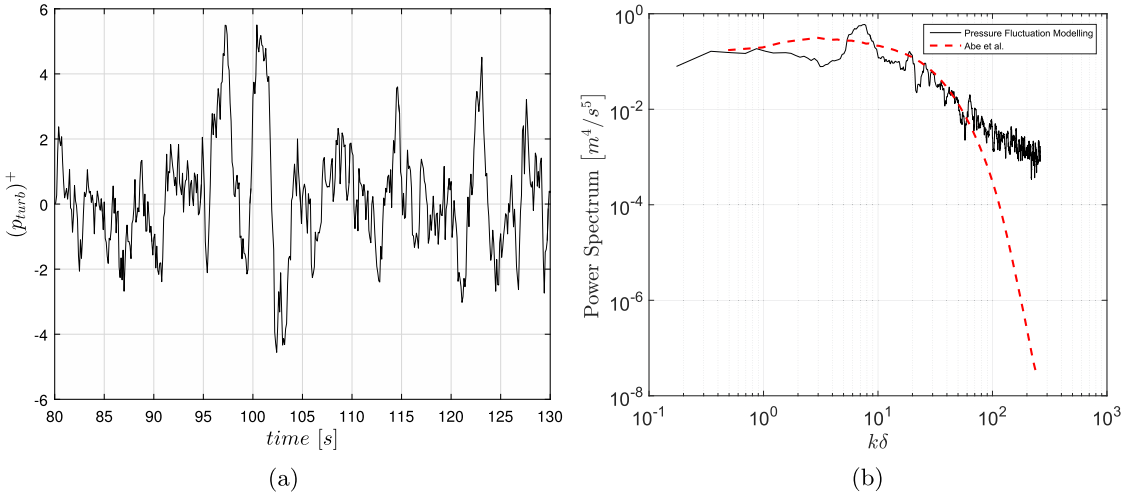

Fig. 5. Figure on the left shows a portion of the normalized turbulent pressure fluctuation, $(p_{turb})^+$ signal from $t = 80$ s to $t = 130$ s at half channel height. Figure on the right shows the comparison between the Power Spectrum Density of turbulent pressure field p' from DNS (Abe et al., 2001) and the PFM.

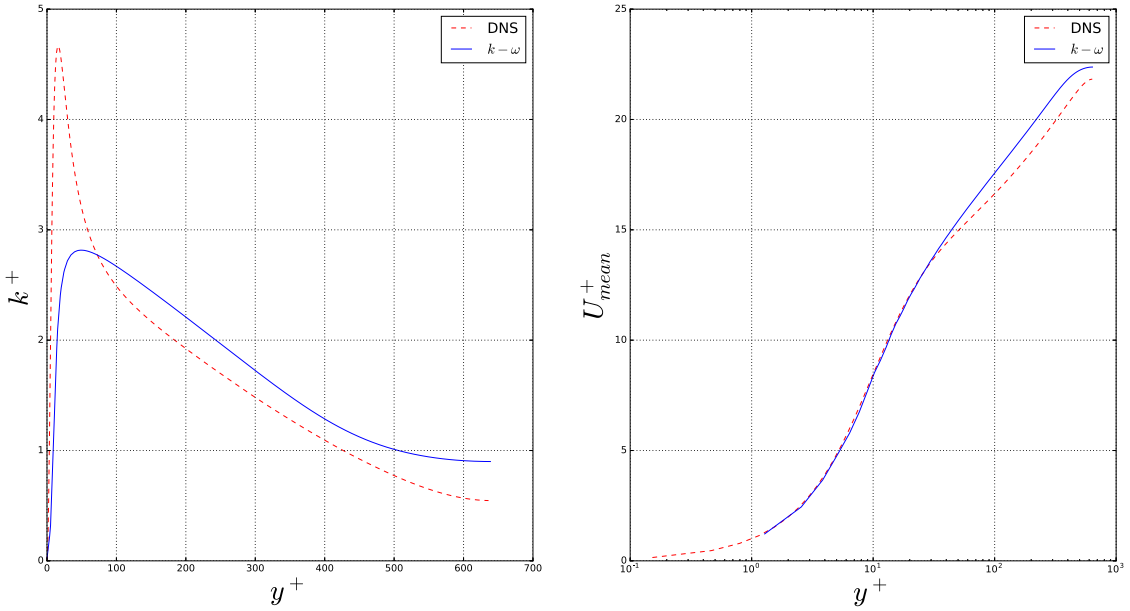

Fig. 6. Comparison between the k^+ and U^+_{mean} plots from the $k-\omega$ U-RANS model and DNS by Abe et al. (2001).

From the above discussion it can be concluded that pressure fluctuation model is sensitive to the results from U-RANS but it shows a good promise to be used in an FSI solver. The sensitivity of the PFM to factors such as the mesh and time-steps can be further studied by performing more FSI simulations.

4.2. Steel flap in turbulent water flow

Based on the conclusions made in the previous section, the model can be further tested in an FSI simulation through a two-way coupling between the PFM based fluid solver to a structure solver. Hence in the second test case the PFM is used in an FSI simulation to estimate the behaviour of flexible steel flap when subjected to turbulent flow across it. The steel flap in a turbulent water case is a variation of the numerical benchmark test case performed by Turek and Hron (2006). This is a 2-dimensional numerical test case consisting of a cantilever steel flap with the same orientation as the fluid flow. The fluid flow (water) around the flap is turbulent in nature. The turbulent flow around the flap leads to fluctuation of pressure on the flap surface causing it to vibrate. This case performed tests the stability and feasibility of using the PFM in an FSI problem to simulate Turbulent Induced Vibrations (TIV).

4.2.1. Simulation set-up

Fig. 7 gives a clear picture of the mesh and the domain size that was used for the simulating TIV. The left and right boundaries of the fluid domain are taken as the inlet and outlet, respectively. The top and bottom boundaries of the domain are walls with no-slip boundary condition. The FSI-interface between the fluid and solid domain is treated as a deformable wall, which conforms with the walls of the steel flap. The relative velocity between the fluid and the wall of the steel flap is set to be zero (which is also a no-slip boundary condition). The average velocity of water is 3 m/s is given as the boundary condition at the inlet and the outlet of the domain is a given a fixed pressure boundary condition with gauge-pressure of 0 *Pa*. The bulk Reynolds Number of the flow is 1.2×10^6.

The steel flap is a 2-dimensional cantilever beam, depicted by the mesh in black color in Fig. 7. The left end of the steel flap is given the Dirichlet boundary condition with zero displacement in all the directions. The other surface patches of the mesh of the steel flap are free to move. The compatibility condition of displacement and velocity is imposed at the fluid–structure interface of the fluid domain. The mesh of the fluid and solid domains are non conformal, therefore a spatial interpolation between the data at the FSI-interface is performed with the help of Radial Basis Functions. The working fluid used here is water and the solid is steel, the properties of both are mentioned in Table 3.

The simulation is performed by two-way coupling of an FVM code OpenFOAM-extend (OpenFOAM, 2013) and the FEM code `Deal.II`. The temporal coupling between the solid and the fluid domains is performed by IQN-ILS method(Interface Quasi Newton with Inverse Jacobian estimate by Least Squared Method) (Degroote, 2013).

Table 3
Material properties used in flexible steel flap in water experiment.

Fluid Properties (Water)	
Density (ρ_f)	1000 kg/m^3
Kinematic Viscosity (ν_f)	1×10^{-6} m^2/s
Structural Properties (Steel)	
Density (ρ_s)	7850 kg/m^3
Elasticity Modulus	210 GPa
Poisson Ratio	0.33

The fluid solver is using the standard $k-\omega$ U-RANS model. At the walls, both moving and fixed; wall functions were used for the turbulent kinetic energy (k) and the turbulent dissipation rate (ω). For the purpose of comparison two cases are performed, the reference case is performed without the use of pressure fluctuation modeling, and the test case is performed with the use of pressure fluctuation modeling. The results are then compared and analyzed. The simulation was performed for a total simulation time of over 8 s with a time step of 0.0005 s for the test and the reference case. The displacements at eh free end of the steel flap were plotted and compared.

4.2.2. Results and discussion

Fig. 8 shows the comparison between the vertical displacements of the free-end of the cantilever beam for the two cases performed. It can be observed that for the reference case, a large initial displacements observed due to the developing flow along the beam, after which the beam vibrations are significantly damped out, and the vibrations in the order of 10^{-6} m are observed. This behavior closely resembles the results of the study performed by ter Hofstede et al. (2017), Santis and Shams (2017), de Ridder et al. (2013) where a standard U-RANS model was used. The absence of fluctuating pressure fields in U-RANS models causes the system to reach a steady state behaviour. However, when the pressure fluctuation model is used alongside the U-RANS model, it can be observed the amplitude of the vibrations induced on the beam is one order of magnitude higher and self-sustaining. The natural frequency and amplitude of the vibrations and are analyzed and tabulated in Table 4. This behaviour is achieved due to a continuous high frequency excitation provided by pressure fluctuations on the steel flap. Hence, the pressure fluctuation models the external excitation source on the steel flap which simulates the effect of TIV.

It can be concluded that both the methods predict the natural frequencies of the beam accurately, which is in conjunction with the studies performed by ter Hofstede et al. (2017), de Ridder et al. (2013). However, with standard U-RANS model, effect of high frequency pressure fluctuations cannot not be simulated due to Reynolds averaging. However, by enabling PFM it is possible to

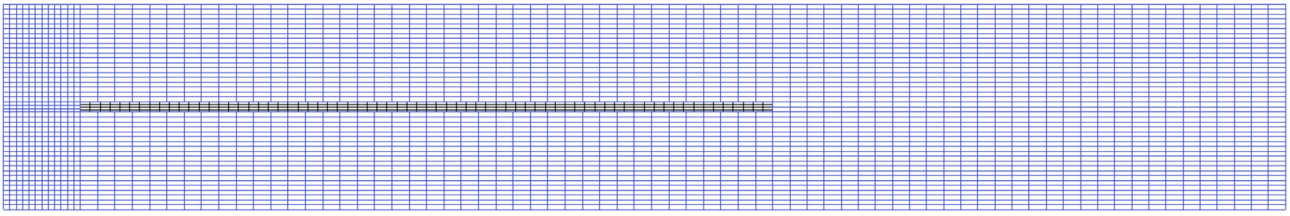

Fig. 7. Mesh and domain of the Steel Flap in Turbulent Water test case. The length of the fluid domain (in blue) $L = 2.5$ m, height of the fluid domain $H = 40$ mm, length of the flap (in black) $l = 1.35$ m and the width of the flap $h = 0.2$ mm.

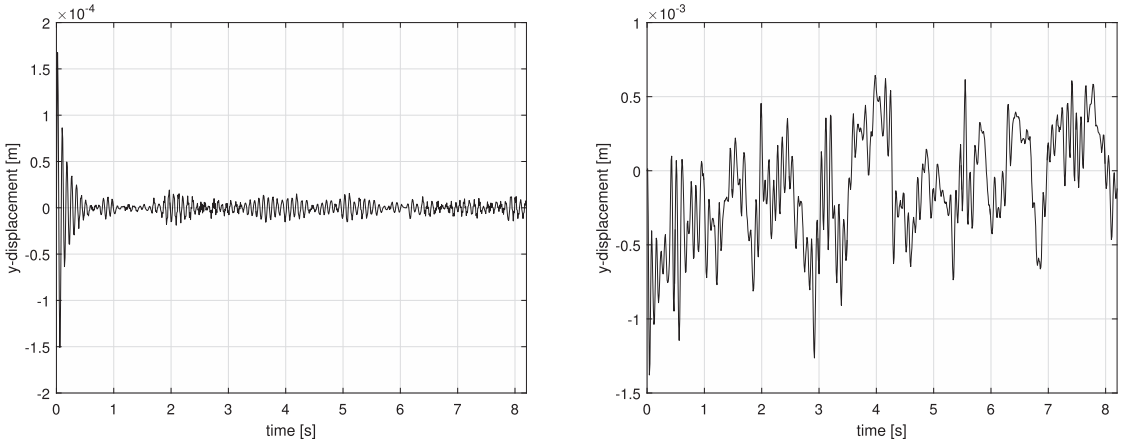

Fig. 8. Comparison between the Vertical displacements of the free-end of the beam obtained from the FSI simulations, without (left) and with (right) the pressure fluctuation model enabled.

Table 4
Comparison of the calculated modal frequency of the systems by calculated by DFFT (Discrete Fast Fourier Transforms).

Case	Modal Frequency [Hz]	RMS Amplitude [mm]
Standard $k-\omega$	12.13	0.014
Pressure Fluctuation Model	12.25	0.379

estimate the amplitudes of vibrations in the structures caused due to high frequency pressure fluctuations and which provides the possibility of investigating the behavior of structures when higher frequency modes are excited or during resonance.

4.2.3. Sensitivity study

To get a better understanding of the impact of mesh and time-steps on the results obtained by further analysis of the flexible flap case through a sensitivity study with respect to mesh and time steps. The mesh sensitivity study is performed by refining the fluid mesh and analyzing the variations in the RMS vertical displacement of the free end of the steel flap. The simulations are performed with $k-\omega$ U-RANS model and the boundary conditions are kept similar to the case performed above. The mesh refinement is performed only on the fluid mesh in exponential factors of 2 ranging from 2^0 to 2^2. The time-steps used for mesh refinement study cases are maintained constant. From the results obtained it is observed that the RMS displacements show a variation of 10% between coarsest and the finest mesh. The variation are observed to decrease with successive mesh refinements and would eventually be asymptotic in nature. The mesh sensitivity of the results are due to a combination of numerical errors during mesh interpolation between fluid and structure meshes and the errors during spatial discretization within the fluid solver.

Similarly a sensitivity study for the PFM solver was performed to check the effect of time steps on the results of the FSI simulations. Three simulations were performed with time steps ranging from 10^{-6} s to 0.001 s. It is observed that the with lower time steps, the variation in the results start decreasing. The sensitivity of the results to time steps can be attributed to numerical errors and discretization schemes.

Although the model succeeds at generating the desired behaviour of the structure, it is yet to be validated with experimental

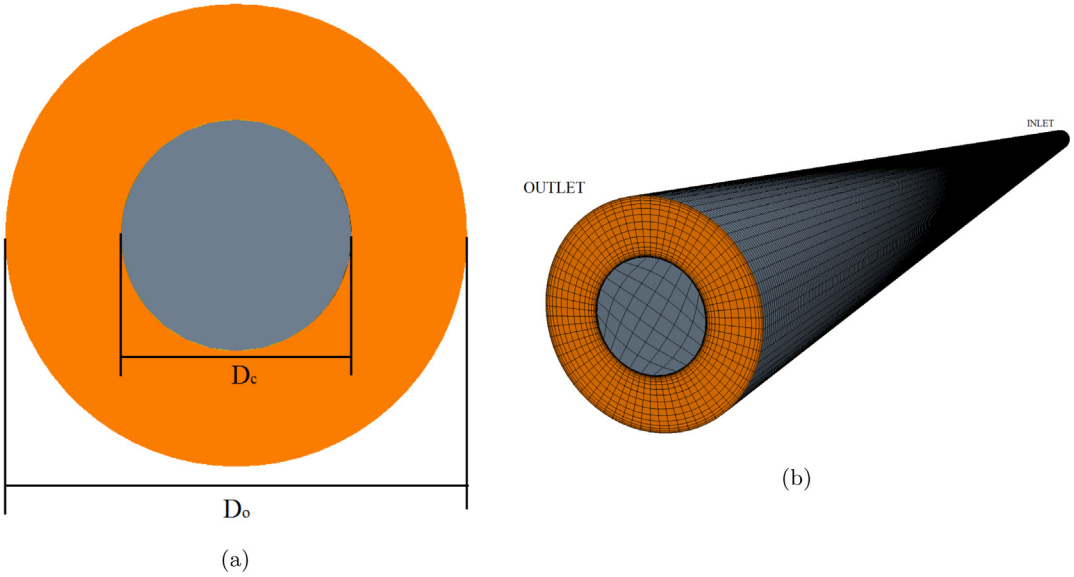

Fig. 9. Geometry of the domain for the flexible beam in water experiment.

cases. For further validation of the model, a third case is performed for comparison between experimental and numerical simulation of TIV by the use of PFM.

4.3. Flexible brass beam in turbulent water

The third numerical test case to validate the pressure fluctuation model is an application based experimental case involving a flexible beam in turbulent water flow by Chen and Wambsganns (1972). The experiment was performed to study the effects of a turbulent flow of water along on a cylindrical brass beam in a rigid container. Similar to the test cases performed before the study focuses on the effect of turbulent flow on slender flexible structures within a confined enclosure. The experimental set-up consists a flexible brass rod, enclosed inside of a rigid steel cylinder. The axis of the outer cylinder is aligned with that of the inner brass rod, and are suspended vertically to avoid gravitational effects. The beam is clamped (fixed) on both the ends (at the inlet and the outlet of the fluid domain). The beam has a core diameter of $D_c = 0.0127$ m and steel outer wall has an outer diameter of, $D_o = 0.0254$ m. the length of the cylinder is $L = 1.19$ m. The geometry of the domain can be shown in Fig. 9. The turbulent flow of water induced vibrations onto the brass rod. In the article by Chen and Wambsganns (1972) the amplitude of vibration of the rod is measured at the beam center and studied to compare it with analytical models. The experiment mimics the behaviour of a single fuel rod when subjected to a turbulent parallel-fluid flow as observed in most nuclear reactors. This application based test case therefore showcases the capabilities of the pressure fluctuation model to simulate real world problems. The objective of the numerical test case is to simulate the experiment performed by Chen and Wambsganns (1972) and validate the pressure fluctuation model by comparing the results of the experiment to the simulation.

Table 5
Material properties used in flexible beam in water experiment.

Fluid Properties (Water)	
Density (ρ_f)	1000 kg/m^3
Kinematic Viscosity (ν_f)	1×10^{-6} m^2/s
Structural Properties (Brass)	
Density (ρ_s)	8400 kg/m^3
Elasticity Modulus	107 GPa
Poisson Ratio	0.331

Table 6
Compiled results for experimental results and the simulated results.

Case	Modal Frequency [Hz]	Amplitude RMS [mm]
Experimental	27.9	0.005
$k-\omega$ SST with PFM	26.0	0.001
$k-\omega$ SST wo PFM	26.0	2e−05

4.3.1. Simulation set-up

The fluid domain for the simulation consists of an annular cylindrical structure with 4 surfaces namely, the inlet, outlet, inner wall and the outer wall. The outer-wall is the rigid steel cylinder, and the inner-wall is the outer surface of the brass beam. The inlet and outlet surfaces are shown in Fig. 9. The inlet of the fluid domain is meshed with quadrilateral cells which is extruded in the direction of outlet of the fluid domain. The outer wall of the fluid domain is rigid (non-deforming), whereas the inner wall of the fluid domain (FSI interface), is allowed to deform to conform with the surface of the brass beam. The wall first cell thickness of the mesh is maintained at $y^+ \geqslant 30$.

The solid domain (brass-rod), consists of 3 surfaces namely, the FSI-interface and the 2 ends of the rod. Similar to the fluid domain, the brass beam is also meshed with tetrahedral cells. A mesh sensitivity study for the beam mesh is performed prior to the simulation. Similar number of mesh points are kept at the FSI interface of the fluid and solid domains to minimize interpolation errors.

The FSI simulation was performed with water as the working fluid. An average inlet velocity of 10 m/s is provided as the boundary condition inlet, and the zero gauge-pressure is provided as a boundary condition at the outlet of the fluid domain. The $k-\omega$ (Wilcox, 1988) U-RANS model was selected for the simulating

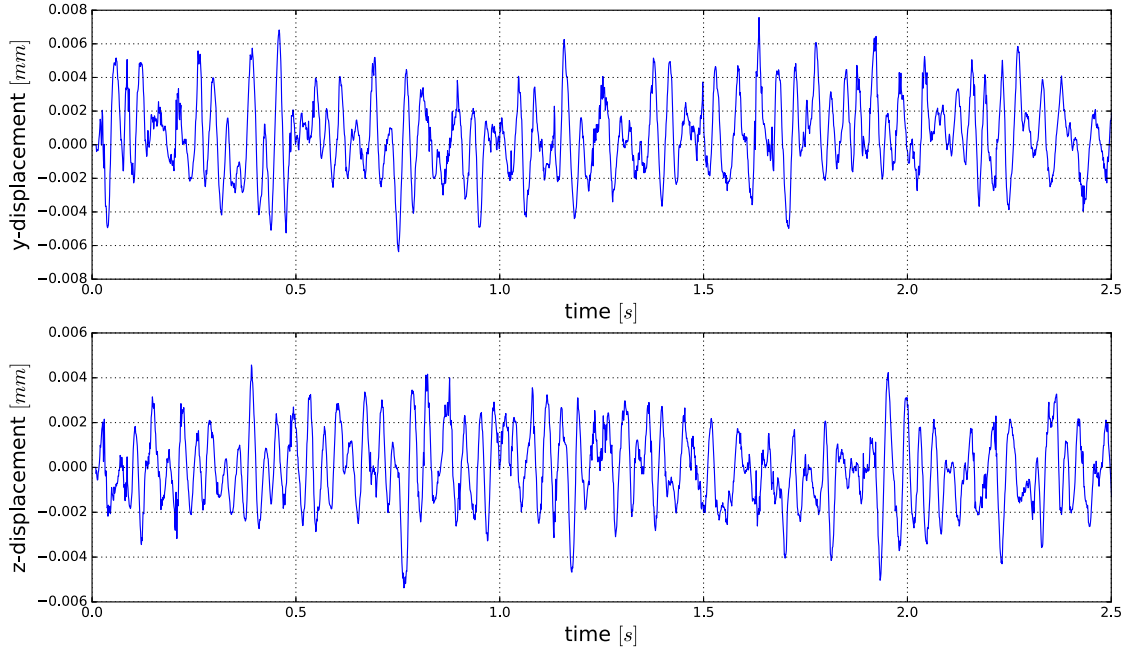

Fig. 10. Displacement vs time signal of the beam center obtained from applying the PFM to FSI solver.

the average turbulent flow. For a fair comparison two cases were performed, the test case with the PFM enabled to act as an external source of excitation to the brass beam; and the second being the reference case with PFM disabled and using the standard U-RANS model. The turbulence intensity at the inlet of the domain is set to 5% with a turbulent length scale of 0.1 cm. Wall functions were used for k and ω for the simulation. Material properties of water and the brass beam used in the FSI simulation, are shown in Table 5. The brass beam is given a fixed–fixed (zero-displacement) boundary condition at both the ends of the beam, similar the condition in the experiment.

An implicit 2^{nd} order temporal scheme is employed to solve the fluid and solid solver. The time step is adjusted to maintain the average Courant number $\leqslant 5$. A two way coupling of the solvers are performed using the IQN-ILS (Degroote, 2013) coupling method re-using 4 time step data to ensure stability and faster convergence of the solver. A higher-order interpolation scheme was used between the mesh of both the domains to minimize the errors due to temporal and spatial interpolation during the coupling iterations. The displacement signal of the brass beam center with respect to time is recorded and analyzed to calculate the required values for comparison with the experiments (Chen and Wambsganns, 1972).

4.3.2. Results and discussion

The amplitude of the vibrations at the beam center is recorded and analyzed. The results obtained have been tabulated in the Table 6. The displacement signal obtained from the applying the PFM in the FSI solver can be observed in the Fig. 10.The frequency analysis show that an error of 7% for the modal frequency when compared to the results by Chen and Wambsganns (1972). A mesh sensitivity study to investigate the error in the beam modal frequencies does not provide a conclusive evidence for the deviation observed.

The results obtained shows the RMS amplitudes from the PFM is observed to be 5 times less compared to experimental values. Also the RMS amplitudes between the PFM model and the experimental case shows that the amplitudes predicted are of the same order of magnitude, however, a difference of two orders of magnitude can be observed when compared to a standard U-RANS model without enabling PFM. This provides a certain degree of confidence on the results obtained by the model.

The simulation therefore suggests that PFM can replicate the behavior similar to that of turbulent flows for FSI solvers.

5. Conclusions

This article focuses on a method to simulate TIV through U-RANS models using the Pressure Fluctuation Model. The article explains the calculations involved in the modeling of turbulent pressure fluctuations. The turbulent pressure fluctuations act as an external excitation causing TIV. The model focuses on the usage of isotropic turbulence assumption.

To validate the method, an initial test case of a turbulent plane channel flow was performed with $Re_\tau = 640$ and compared to DNS results of Abe et al. (2001). It is observed that the RMS value of pressure fluctuations modeled are in the same order of magnitude when compared to the DNS. The modeled pressure fluctuations is later used as an external source of excitation for the structure to simulate TIV.

After validating the model with a fluid only test case, an FSI problem to simulate TIV is performed as the next step. A 2-dimensional numerical test case is chosen. The test case consists of a 2-dimensional cantilever steel flap in turbulent water flow, with the flow being along the longitudinal axis. This test case was performed using U-RANS model, with and without the use of pressure fluctuation model. The results of these two cases were then compared to check the difference caused by the PFM on the results. It is observed that the standard U-RANS model without pressure fluctuation model leads to damping of the vibrations of the beam due to lack of excitation from the fluid solver. However when using the PFM the additional excitation from the estimated turbulent pressure fluctuations the vibrations are self-sustaining. A sensitivity study is also performed to check the variation of results with mesh and time steps. No significant variations were observed and an asymptotic behaviour in both the cases.

Finally a 3-dimensional experimental case was simulated to validate the model. The experimental case by Chen and Wambsganns (1972) was simulated to compare the effect of turbulent fluctuating fields on a flexible brass beam. The results obtained shows the RMS amplitudes from the PFM is observed to be 5 times less compared to experimental values. However, the RMS amplitude of the beam vibrations are of the same order of magnitude as the experiment as compared to a standard U-RANS model which is 2 orders of magnitude lower compared to experimental results. This proves its feasibility of use.

In conclusion, the initial results obtained from Section 4.2 shows that enabling PFM within a fluid solver simulates the turbulent pressure at the fluid–structure interface at each time step which triggers a vibrations on the flexible structures similar to that observed in TIV. However, the method is not an exact estimation of turbulent pressure fluctuations and there is further scope of improvement in the results to be used in FSI problems. Also, further investigation has to made on the stability of this model for stronger FSI problems.

Acknowledgements

The work described in this paper is funded by the Dutch Ministry of Economic Affairs. The authors would like to acknowledge the work of David S. Blom for his contribution in coupling of the fluid and structure codes.

Appendix A. Supplementary data

Supplementary data associated with this article can be found, in the online version, athttps://doi.org/10.1016/j.anucene.2019.01.001.

References

Abe, H., Kawamura, H., Matsuo, Y., 2001. Direct numerical simulation of a fully developed turbulent channel flow with respect to the reynolds number dependence. ASME J. Fluids Eng. 2, 382–393. https://doi.org/10.1115/1.1366680.

Arndt, D., Bangerth, W., Davydov, D., Heister, T., Heltai, L., Kronbichler, M., Maier, M., Pelteret, J.P., Turcksin, B., Wells, D., 2017. The Deal.II library, version 8.5. J. Numer. Math. https://doi.org/10.1515/jnma-2016-1045.

Blevins, R., 1979. Flow-induced vibration in nuclear reactors: a review. Prog. Nucl. Energy 4, 25–49. https://doi.org/10.1016/0149-1970(79)90008-8.

Chase, D., 1980. Modeling the wavevector-frequency spectrum of turbulent boundary layer wall pressure. J. Sound Vib. 70, 29–67. https://doi.org/10.1016/0022-460x(80)90553-2.

Chase, D., 1987. The character of the turbulent wall pressure spectrum at subconvective wavenumbers and a suggested comprehensive model. J. Sound Vib. 112, 125–147. https://doi.org/10.1016/s0022-460x(87)80098-6.

Chen, S.S., Wambsganns, M.W., 1972. Parallel flow induced vibration of fuel rods. Nucl. Eng. Des. 18, 253–278.

Conner, M.E., Baglietto, E., Elmahdi, A.M., 2010. CFD methodology and validation for single-phase flow in PWR fuel assemblies. Nucl. Eng. Des. 240, 2088–2095. https://doi.org/10.1016/j.nucengdes.2009.11.031.

Degroote, J., 2013. Archives of computational methods in engineering. In: chapter Partitioned Simulation of Fluid-Structure Interaction, Coupling Black-Box Solvers with Quasi-Newton Techniques. Springer International Publishing.

de Ridder, J., Degroote, J., Tichelen, K., Schuurmans, P., 2013. Modal characteristics of a flexible cylinder in turbulent axial flow from numerical simulations. J. Fluids Struct. 43, 110–123.

Hinze, J.O., 1975. Turbulence,. McGraw-Hill.
JSME, 2008. Flow Induced Vibrations. Elsevier.
Juvé, D., Berton, M., Salze, E., 2014. Spectral properties of wall-pressure fluctuations and their estimation from computational fluid dynamics. In: Flinovia – Flow Induced Noise and Vibration Issues and Aspects. Springer International Publishing, pp. 27–46. https://doi.org/10.1007/978-3-319-09713-8_2.
OpenFOAM, 2013. User Guide, Version 2.2.0. OpenFOAM Foundation.
Païdoussis, M., 1983. A review of flow induced vibrations in reactor and reactor components. Nucl. Eng. Des. 74, 31–60.
Païdoussis, M., Curling, L., 1985. An analytical model for vibration of clusters of flexible cylinders in turbulent axial flow. J. Sound Vib. 98, 493–517. https://doi.org/10.1016/0022-460x(85)90258-5.
Païdoussis, M.P., Gagnon, J.O., 1984. Experiments on vibration of cluster of cylinders in axial flow: modal and spectral characteristics. J. Sound Vib. 96, 341–352.
Peltier, L., Hambric, S., 2007. Estimating turbulent-boundary-layer wall-pressure spectra from CFD RANS solutions. J. Fluids Struct. 23, 920–937. https://doi.org/10.1016/j.jfluidstructs.2007.01.003.
Pope, S.B., 2000. Turbulent Flows. Cambridge University Press. https://doi.org/10.1017/cbo9780511840531.
Santis, D.D., Shams, A., 2017. Numerical modeling of flow induced vibration of nuclear fuel rods. Nucl. Eng. Des. 320, 44–56. https://doi.org/10.1016/j.nucengdes.2017.05.013.
Santis, D.D., Kottapalli, S., Shams, A., 2018. Numerical simulations of rod assembly vibration induced by turbulent axial flows. Nucl. Eng. Des. 335, 94–105. https://doi.org/10.1016/j.nucengdes.2018.04.027.
Santis, D.D., Shams, A., 2019. Analysis of flow induced vibrations and static deformations of fuel rods considering the effects of wire spacers and working fluids. J. Fluid. Struct. 84, 440–465.
Senthooran, S., 2002. A Computational Model to Calculate Flow-Induced Pressure Fluctuations on a Bluff Body Ph.D. thesis. Texas Tech University.
Senthooran, S., Lee, D.-D., Parameswaran, S., 2004. A computational model to calculate the flow-induced pressure fluctuations on buildings. J. Wind Eng. Ind. Aerodyn. 92, 1131–1145. https://doi.org/10.1016/j.jweia.2004.07.002.
Tennekes, H., Lumley, J.L., 1972. A First Course in Turbulence. The MIT Press.
ter Hofstede, E., Kottapalli, S., Shams, A., 2017. Numerical prediction of flow induced vibrations in nuclear reactor applications. Nucl. Eng. Des. 319, 81–90. https://doi.org/10.1016/j.nucengdes.2017.04.026.
Turek, S., Hron, J., 2006. Proposal for numerical benchmarking of fluid-structure interaction between an elastic object and laminar incompressible flow. In: Lecture Notes in Computational Science and Engineering. Springer, Berlin Heidelberg, pp. 371–385. https://doi.org/10.1007/3-540-34596-5_15.
Wilcox, D.C., 1988. Re-assessment of the scale-determining equation for advanced turbulence models. AIAA J.